

# Phase Transitions in the Metastable Perovskite Multiferroics $\text{BiCrO}_3$ and $\text{BiCr}_{0.9}\text{Sc}_{0.1}\text{O}_3$ : A Comparative Study

João Pedro Cardoso, Davide Delmonte, Edmondo Gilioli, Elena L. Fertman, Alexey V. Fedorchenko, Vladimir V. Shvartsman, Vaidotas Paukšta, Robertas Grigalaitis, Jūras Banys, Dmitry D. Khalyavin, Joaquim M. Vieira, and Andrei N. Salak\*



Cite This: *Inorg. Chem.* 2020, 59, 8727–8735



Read Online

ACCESS |



Metrics & More

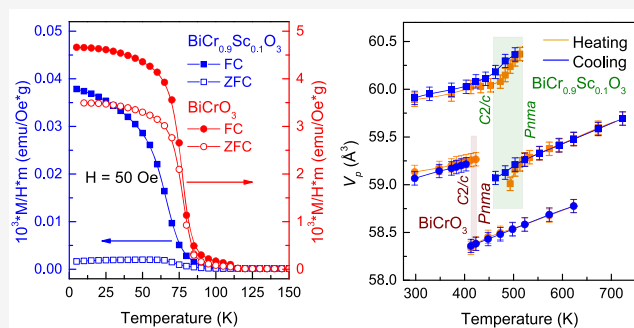


Article Recommendations



Supporting Information

**ABSTRACT:** The temperature behavior of the crystal structure as well as dielectric and magnetic properties of the perovskite bismuth chromate ceramics with the 10 mol %  $\text{Cr}^{3+}$ -to- $\text{Sc}^{3+}$  substitution were studied and compared with those of the unmodified compound. Using a high-pressure synthesis,  $\text{BiCrO}_3$  and  $\text{BiCr}_{0.9}\text{Sc}_{0.1}\text{O}_3$  were obtained as metastable perovskite phases which are monoclinic  $C2/c$  with the  $\sqrt{6}a_p \times \sqrt{2}a_p \times \sqrt{6}a_p$  superstructure (where  $a_p$  is the primitive perovskite unit-cell parameter) under ambient conditions. At room temperature, the unit cell volume of  $\text{BiCr}_{0.9}\text{Sc}_{0.1}\text{O}_3$  is  $\sim 1.3\%$  larger than that of  $\text{BiCrO}_3$ . Both perovskites undergo a reversible structural transition into a nonpolar  $\text{GdFeO}_3$ -type phase (orthorhombic  $Pnma$ ,  $\sqrt{2}a_p \times 2a_p \times \sqrt{2}a_p$ ) in the temperature ranges of 410–420 K ( $\text{BiCrO}_3$ ) and 470–520 K ( $\text{BiCr}_{0.9}\text{Sc}_{0.1}\text{O}_3$ ) with a relative jump of the primitive perovskite unit cell volume of about  $-1.6$  and  $-2.0\%$ , respectively. Temperature dependences of the complex dielectric permittivity demonstrate anomalies in the phase transition ranges. The  $Pnma$ -to- $C2/c$  crossover in  $\text{BiCrO}_3$  is accompanied by a decrease in the direct current (dc) conductivity, while in  $\text{BiCr}_{0.9}\text{Sc}_{0.1}\text{O}_3$  the conductivity increases. The onset of an antiferromagnetic order in  $\text{BiCr}_{0.9}\text{Sc}_{0.1}\text{O}_3$  is observed at the Néel temperature ( $T_N$ ) of about 85 K as compared with  $T_N = 110$  K in  $\text{BiCrO}_3$ . In contrast to  $\text{BiCrO}_3$ , which exhibits a spin reorientation at  $T_{sr} \sim 72$  K, no such a transition occurs in  $\text{BiCr}_{0.9}\text{Sc}_{0.1}\text{O}_3$ .



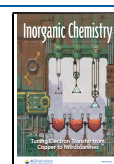
## 1. INTRODUCTION

Perovskite-like materials are known for their various prominent properties, such as piezoelectricity,<sup>1</sup> colossal magnetoresistance,<sup>2</sup> multiferroicity,<sup>3</sup> photoelectric activity,<sup>4</sup> or superconductivity.<sup>5</sup> Besides, their relatively simple structures derived from the primitive cubic prototype  $Pm\bar{3}m$  allow one to interpret and perform theoretical studies on the occurrence of those properties. Oxide perovskites are the most studied: By now, virtually all of the promising  $\text{ABO}_3$  compositions have been tested and (if possible) produced using the conventional preparation methods.<sup>6</sup> In a number of cases, the desired composition could not be obtained as a single perovskite phase. A high-pressure (HP) synthesis technique applied to the preparation of perovskite phases in the late 1960s overcomes some limitations of the conventional routes and expands the range of possible chemical  $\text{ABO}_3$  combinations.<sup>7,8</sup> This method allows obtaining crystalline phases in a metastable equilibrium upon quenching from HP and high-temperature conditions. Under HP,  $\text{ABO}_3$  compositions tend to crystallize in the most compact structure, such as the perovskite one. Formation of the perovskite phase can occur via either a polymorph transformation from a less close-packed structure

or a direct synthesis from simpler oxides when no single composition can be obtained at ambient conditions. The HP synthesis enables the stabilization of particular oxidation states of cations and configurations with considerable ionic size differences.<sup>8</sup> The most eminent examples of such cases are the quadruple perovskites,  $\text{A}_{1-x}\text{A}_x^{2+}\text{Mn}_3^{3+}\text{Mn}_4\text{O}_{12}$ ,<sup>9</sup> and the A-site ordered perovskites  $\text{AA}'_3\text{B}_4\text{O}_{12}$  ( $\text{A}' = \text{Cu}^{2+}$ ),<sup>10</sup> respectively. These and other compositions stabilized under high pressure offer interesting structures with unique combinations of orderings and distortions. Solid solution series<sup>11</sup> and series of isomorphous substitutions,<sup>12</sup> in which one or more members is an HP-stabilized perovskite, offering a good basis for understanding of regularities of structural variations, as well as magnetic and dielectric behaviors in terms of size and electronic configuration of the constituent cations.

Received: February 2, 2020

Published: June 9, 2020



Among multifunctional compounds with a perovskite-like structure, materials that combine at least two of three ferroic order parameters, so-called multiferroics, have attracted great attention. BiCrO<sub>3</sub> is one of the first HP synthesized perovskite multiferroics, which has been well-documented and studied.<sup>13–16</sup> Bismuth chromate stabilizes in the centrosymmetric monoclinic C2/c modification with the  $\sqrt{6}a_p \times \sqrt{2}a_p \times \sqrt{6}a_p$  superstructure (where  $a_p$  is the primitive perovskite unit-cell parameter), which undergoes a reversible phase transition at 410 K to the nonpolar GdFeO<sub>3</sub>-type orthorhombic Pnma phase ( $\sqrt{2}a_p \times 2a_p \times \sqrt{2}a_p$ ).<sup>14</sup> Niitaka et al. reported an anomaly of the dielectric permittivity associated with this phase transition.<sup>13</sup> They also indicated a parasitic ferromagnetic ordering below 114 K, which was then identified by Darie et al.<sup>15</sup> as a weak spontaneous magnetic moment associated with a G-type antiferromagnetic order.

The second end member of the virtual perovskite solid solution system BiCr<sub>1-x</sub>Sc<sub>x</sub>O<sub>3</sub>, bismuth scandate, also exists in bulk form only as a HP-stabilized phase.<sup>17</sup> The as-prepared phase is the monoclinic C2/c one ( $\sqrt{6}a_p \times \sqrt{2}a_p \times \sqrt{6}a_p$ ) at room temperature. However, as opposed to BiCrO<sub>3</sub>, the thermal treatment of BiScO<sub>3</sub> results in the irreversible phase transition from the monoclinic to the antipolar orthorhombic Pnma polymorph ( $\sqrt{2}a_p \times 4a_p \times 2\sqrt{2}a_p$ ) above about 700 K.<sup>18</sup>

The interest in a chrome-to-scandium substitution in BiCrO<sub>3</sub> was driven by the impressive results of the study of annealing behavior of the HP-stabilized perovskite phases in the BiFeO<sub>3</sub>–BiScO<sub>3</sub> solid solution series.<sup>19</sup> Khalyavin et al.<sup>18</sup> have shown that practically the whole series demonstrates the annealing stimulated polymorphism with three compositional ranges, where distinct metastable polymorphs with novel ferroelectric and antiferroelectric perovskite structures with interesting magnetic properties form. Such behavior, referred to as *conversion polymorphism*, was suggested to be a general phenomenon that can be found in other HP-stabilized materials.

Here we report on HP synthesis of metastable perovskite phases of the BiCr<sub>1-x</sub>Sc<sub>x</sub>O<sub>3</sub> series ( $x = 0$  and 0.1) and a comparative study of the temperature behavior of their crystal structure as well as dielectric and magnetic properties. The goal of this work was 2-fold. First, a partial substitution of Cr<sup>3+</sup> by considerably bigger Sc<sup>3+</sup> was expected to increase distortions and thereby modify properties of bismuth chromate without changes in the crystal structure symmetry (since BiCrO<sub>3</sub> and BiScO<sub>3</sub> are both monoclinic with the same C2/c space group). Second, it was supposed that a comparative analysis of the temperature behavior of the crystal structure, dielectric response, and magnetic ordering of BiCrO<sub>3</sub> and BiCr<sub>0.9</sub>Sc<sub>0.1</sub>O<sub>3</sub> can help to understand better the nature of ferroic orders in the unmodified bismuth chromate.

## 2. EXPERIMENTAL SECTION

Bismuth(III) oxide (99.9%, Merck), chromium(III) oxide (99.9%, Merck), and scandium(III) oxide (99.9%, Abcr) were used as starting materials. The reagents were mixed and ground in stoichiometric ratios corresponding to the compositions BiCrO<sub>3</sub> and BiCr<sub>0.9</sub>Sc<sub>0.1</sub>O<sub>3</sub> and put in an Au capsule (25 μm thick), inserted into an octahedral MgO cell assembly, and placed in a 6/8-type multianvil Walker-type apparatus (Rockland Research Corp.). The HP synthesis took 2 h at 60 kbar and 1190 K. Pressure was applied at a rate of 65 bar/min followed by a temperature increase (50 K/min). After the synthesis, the sample was quenched to room temperature, and the pressure was slowly released (average rate of –30 bar/min). The temperature was

monitored with a Pt/Pt–Rh10% thermocouple in contact with the sample.

For the phase analysis and the crystal structure characterization, the obtained ceramics were reduced to powders. X-ray diffraction (XRD) studies of the powders were performed using a PANalytical X'Pert MPD PRO diffractometer (Ni-filtered Cu Kα radiation) with an exposition of about 2 s per 0.02° step over a 2-theta range of 10–90°. *In situ* temperature XRD measurements were conducted in an Anton Paar HTK 16N chamber between 300 and 870 K upon both heating and cooling. In consideration of the metastable nature of the materials under study, the samples have dwelled for 30 min at each temperature point before the XRD data collecting to ensure equilibrium condition. The obtained XRD data were refined by the Rietveld method using the FULLPROF suite<sup>20</sup> in the profile matching mode.

Atomic force microscopy and piezoresponse force microscopy (AFM and PFM) studies were performed using a commercial scanning probe microscope MFP-3D (Asylum Research). Pt-coated cantilevers SEIHR with a spring constant of 10 N/m were used. PFM measurements were conducted at probing voltage with an amplitude  $U_{ac} = 10–15$  V and frequency  $f = 50$  kHz. Temperature measurements were performed using a PolyHeater heating stage (Asylum Research).

Annealing behavior of the HP-synthesized ceramics was also investigated *ex situ* followed by scanning electron microscopy (SEM) imaging and XRD analysis. Thermal treatment was carried out at 373 and 423 K and then for every 25 K until 573 K with a 2 h dwell at each temperature point. Heating and cooling rates were 10 K/min. The samples were polished with SiC grinding papers down to 5 μm (for standard SEM observation), followed by diamond paste down to 0.25 μm, finishing with 0.063 μm colloidal silica (for the electron backscatter diffraction, EBSD, analysis). The microstructure of the ceramics was studied using a Hitachi S-4100 SEM operating at 25 kV. The EBSD patterns were registered with a Bruker e-Flash detector coupled to a Hitachi SU-70 SEM, operating at 25 kV. The data was analyzed with the software ESPRIT CrystAlign.

The dielectric response of the ceramics was measured in the range of 40–530 K on cooling with a rate of 1 K/min. The measurements were performed in two frequency ranges, namely, between 20 Hz and 1 MHz, and from 2 MHz to 3 GHz. Correspondingly, an LCR meter HP-4284A and a vector network analyzer Agilent 8714ET in a coaxial line were used.

Magnetic properties of the ceramics were measured as a function of temperature using a noncommercial superconducting quantum interference device (SQUID) magnetometer in both zero-field cooled (ZFC) and field-cooled (FC) modes in a magnetic field of 50 Oe between 5 and 300 K.

## 3. RESULTS AND DISCUSSION

The room-temperature XRD patterns of the as-prepared BiCrO<sub>3</sub> and BiCr<sub>0.9</sub>Sc<sub>0.1</sub>O<sub>3</sub> ceramics were found to demonstrate the same types of splitting of the fundamental reflections (see Figure S1). Therefore, the crystal structure of both compositions was refined using the space group C2/c suggested for the HP-stabilized monoclinic perovskite phase of BiCrO<sub>3</sub>.<sup>14,15</sup> The refinement was successful with the following values of the lattice parameters:  $a = 9.4747(3)$  Å,  $b = 5.4874(4)$  Å,  $c = 9.5989(2)$  Å, and  $\beta = 108.574(2)^\circ$ , and  $a = 9.6088(3)$  Å,  $b = 5.5162(2)$  Å,  $c = 9.5361(3)$  Å, and  $\beta = 108.565(2)^\circ$  for BiCrO<sub>3</sub> and BiCr<sub>0.9</sub>Sc<sub>0.1</sub>O<sub>3</sub>, respectively. The values obtained for the unmodified bismuth chromate are essentially close to those reported previously.<sup>14,15</sup> The BiCr<sub>0.9</sub>Sc<sub>0.1</sub>O<sub>3</sub> composition has the unit cell volume by about 1.3% larger than that of BiCrO<sub>3</sub> due to the partial substitution of chromium by scandium (cf.: the corresponding ionic radii of Cr<sup>3+</sup> and Sc<sup>3+</sup> in the 6-fold coordination are 0.76 and 0.89 Å, respectively).

As temperature is increased, both compositions exhibit a temperature-induced phase transition from the monoclinic C2/c

*c* to the nonpolar orthorhombic *Pnma* phase (Figure S2).  $\text{BiCr}_{0.9}\text{Sc}_{0.1}\text{O}_3$  transforms into the *Pnma* modification in the range of 493–513 K, while the corresponding transition range in  $\text{BiCrO}_3$  is narrower, namely, between 413 and 423 K, which is in agreement with the data reported in the literature.<sup>13–15</sup> The monoclinic-to-orthorhombic transition in both compositions under study is reversible. The *Pnma* to *C2/c* transformation in  $\text{BiCrO}_3$  upon cooling occurs within the same temperature range as that upon heating, while in the Sc-substituted composition, the range of the phase coexistence upon cooling is wider and is shifted to a lower temperature range (463–503 K).

For easy comparison, the refined values of the lattice parameters at each temperature point were recalculated to the values of the primitive perovskite lattice parameters:  $a_p = c_p \neq b_p$ ,  $\alpha_p \neq \beta_p = \gamma_p \neq 90^\circ$  for the monoclinic *C2/c* phase (m) and  $a_p = c_p \neq b_p$ ,  $\alpha_p = \gamma_p = 90^\circ \neq \beta_p$  for the orthorhombic *Pnma* phase (o). The following relations for the basis vectors of the distorted structures and the parent cubic cell were used:  $a_m = 2a_p + b_p + c_p$ ,  $b_m = b_p - c_p$ , and  $c_m = -2a_p + b_p + c_p$ <sup>19</sup> and  $a_o = a_p + c_p$ ,  $b_o = 2b_p$ ,  $c_o = a_p - c_p$ .<sup>21</sup>

The temperature dependencies of the normalized primitive unit-cell volume ( $V_p$ ) of both compositions under study are shown in Figure 1. The  $V_p$  value gradually grows up to the

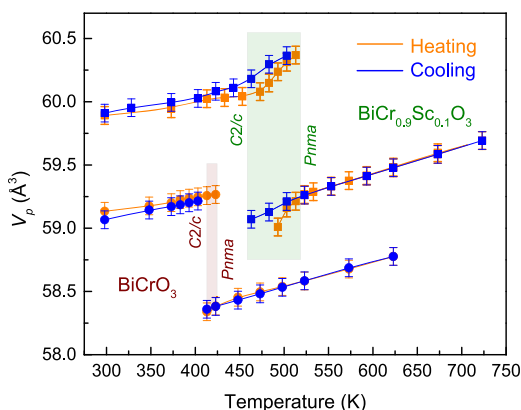


**Figure 1.** Normalized primitive unit cell volume of  $\text{BiCrO}_3$  (solid circles) and  $\text{BiCr}_{0.9}\text{Sc}_{0.1}\text{O}_3$  (solid squares) as a function of temperature, with the phase coexistence (*C2/c* + *Pnma*) ranges indicated with shadow zones.

transition temperature range, where it suddenly drops with a relative change of  $-1.6$  and  $-2.0\%$  for  $\text{BiCrO}_3$  and  $\text{BiCr}_{0.9}\text{Sc}_{0.1}\text{O}_3$ , respectively. While the  $V_p(T)$  behavior of the unmodified bismuth chromate is the same upon heating and cooling, the unit-cell volume of  $\text{BiCr}_{0.9}\text{Sc}_{0.1}\text{O}_3$  changes faster with temperature upon heating than upon cooling (Figure 1). Beyond the transition temperature ranges, the  $V_p(T)$  dependences coincide within the experimental error.

A simple extrapolation of the  $V_p(T)$  dependences of the *Pnma* phase down to room temperature shows that the nonpolar phase in both  $\text{BiCrO}_3$  and  $\text{BiCr}_{0.9}\text{Sc}_{0.1}\text{O}_3$  is more compact than the monoclinic one. It is in agreement with the results of the first-principles calculations, which indicate that the ground structure of  $\text{BiCrO}_3$  is the nonpolar *Pnma* (a  $\text{GdFeO}_3$ -type).<sup>22</sup> Nevertheless, it appears that the monoclinic *C2/c* structure is more favorable below about 410 and 460 K for  $\text{BiCrO}_3$  and  $\text{BiCr}_{0.9}\text{Sc}_{0.1}\text{O}_3$ , respectively.

It follows from comparison of the primitive unit cell parameters of  $\text{BiCrO}_3$  and  $\text{BiCr}_{0.9}\text{Sc}_{0.1}\text{O}_3$  that the substitution of  $\text{Sc}^{3+}$  for  $\text{Cr}^{3+}$  in  $\text{BiCrO}_3$  results in such a change of the pseudomonoclinic primitive perovskite cell that at the  $\alpha_p$ -angle remains near the same (about  $89.2^\circ$ ), while the  $\beta_p$ -angle decreases from  $90.2$  to  $89.9^\circ$ . Both  $a_p$  and  $b_p$  parameters increase and the relative increment of the former is slightly smaller than that of the latter.

The parameters  $\alpha_p$ ,  $\beta_p$  and  $a_p$ ,  $b_p$  as functions of temperature are shown in Figures 2 and 3, respectively. One can see that

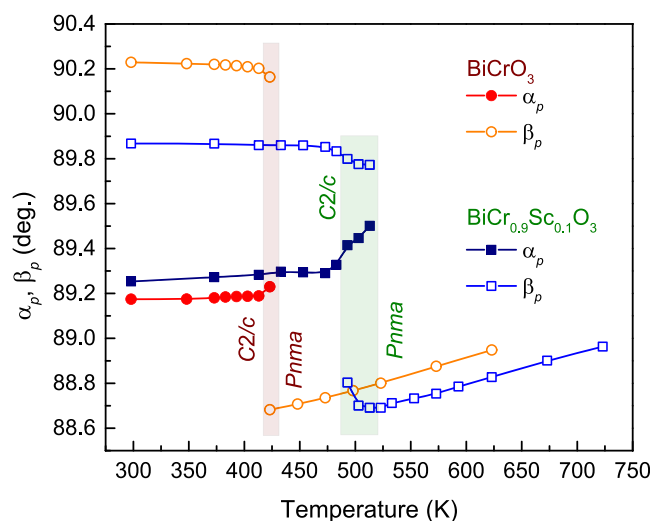


**Figure 2.** Temperature dependencies of the primitive perovskite cell angles,  $\alpha_p$  and  $\beta_p$ , for  $\text{BiCrO}_3$  (circles) and  $\text{BiCr}_{0.9}\text{Sc}_{0.1}\text{O}_3$  (squares) upon heating. The shadow zones indicate the phase coexistence (*C2/c* + *Pnma*) ranges.

the primitive cell angles do not vary much with the increasing temperature until the phase transition range. In the phase coexistence range, the  $\alpha_p$  and  $\beta_p$  values tend to approach each other, followed by a sudden jump of  $\alpha_p$  to  $90^\circ$  (Figure 2).

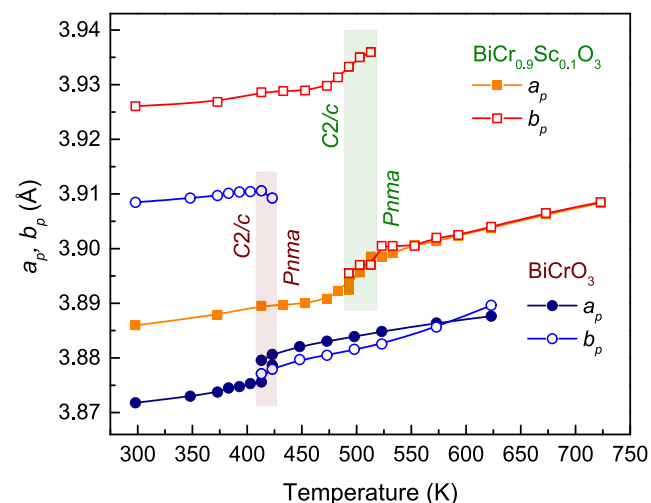


**Figure 3.** Primitive perovskite cell parameters of  $\text{BiCrO}_3$  (circles) and  $\text{BiCr}_{0.9}\text{Sc}_{0.1}\text{O}_3$  (squares) as a function of temperature upon heating. The shadow zones indicate the phase coexistence (*C2/c* + *Pnma*) ranges.

The observed temperature dependence of the parameters  $a_p$  and  $b_p$  is very similar to the  $V_p(T)$  behavior for the respective compositions (cf.: Figures 1 and 3).

Temperature-induced variations in the ceramics surface was monitored *in situ* using AFM. It was revealed that heating the samples above the respective transition temperature ranges led to some irreversible changes in their microstructure. Figure 4

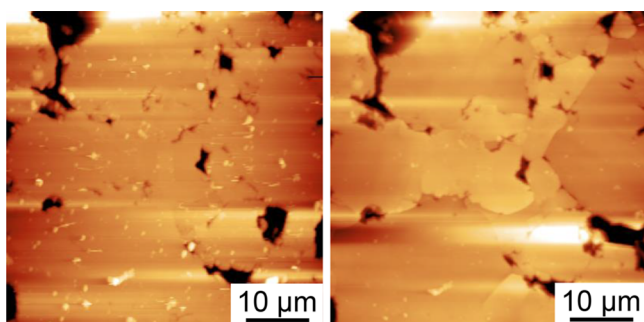


**Figure 4.** Topography AFM images of the  $\text{BiCrO}_3$  ceramics: at room temperature (left) and at 460 K, above the transition temperature (right).

shows the topography images of the polished surface of the  $\text{BiCrO}_3$  ceramics at the temperatures below and above the  $C2/c$ - $Pnma$  phase transition. One can clearly see the grain boundaries and even some cracks (bottom right) developed after transformation into the orthorhombic phase. The modified microstructure was found to remain after reverse transformation upon cooling down to room temperature.

The observed temperature-dependent features motivated a more detailed study of annealing behavior of microstructure of  $\text{BiCrO}_3$  and  $\text{BiCr}_{0.9}\text{Sc}_{0.1}\text{O}_3$ . Figure 5 demonstrates SEM images

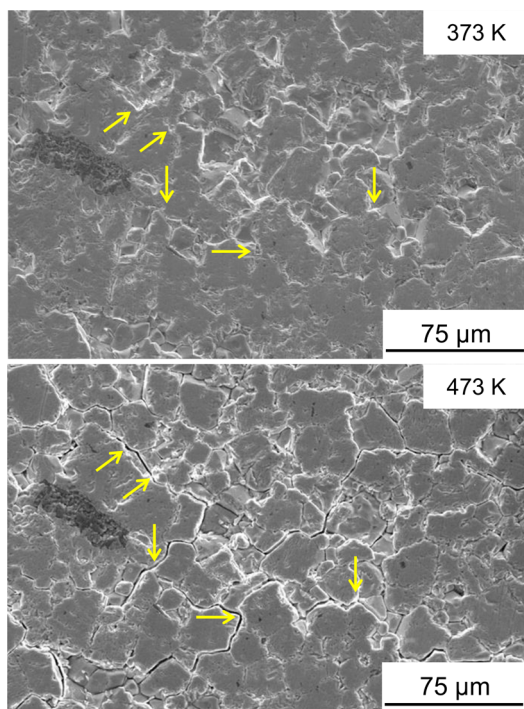


**Figure 5.** SEM images of the  $\text{BiCrO}_3$  ceramic surface after 2 h of annealing at 373 K (top) and 473 K (bottom). The arrows indicate the same microstructural entities in the images.

of the same  $\text{BiCrO}_3$  sample after cumulative annealing treatments with the maximum temperature 373 and 473 K. Intergranular cracks are clearly seen in the ceramics annealed above the transition temperature range (which is 413–423 K for  $\text{BiCrO}_3$  as mentioned before). Such cracking is believed to occur due to the relatively big change in the unit cell volume resulting from the monoclinic-to-orthorhombic phase transition. It should be noticed that the volume change ( $\Delta V_p$ ) at the phase transition upon heating is negative for both  $\text{BiCrO}_3$  and  $\text{BiCr}_{0.9}\text{Sc}_{0.1}\text{O}_3$ . Since a HP-stabilized perovskite phase is usually the most compact structure, it is rather typical to observe phase transitions with a positive  $\Delta V_p$  (at  $\Delta T > 0$ ) in metastable perovskites (see ref 18).

Annealing behavior of the microstructures of  $\text{BiCrO}_3$  and  $\text{BiCr}_{0.9}\text{Sc}_{0.1}\text{O}_3$  was also studied *ex situ* using XRD data. Full width at half-maximum (fwhm) of some fundamental perovskite reflections was measured at room temperature. Figure 6

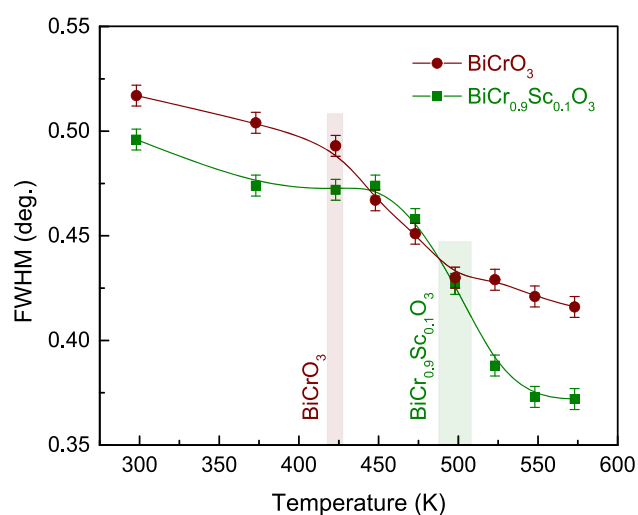


**Figure 6.** The fwhm of the  $(110)_p$  multiplet in the XRD patterns recorded at room temperature for  $\text{BiCrO}_3$  and  $\text{BiCr}_{0.9}\text{Sc}_{0.1}\text{O}_3$  after cumulative annealing treatment as a function of the maximum annealing temperature. The lines are guides for the eyes. The shadow zones correspond to the transition temperature ranges for each composition.

shows the fwhm of the  $(110)_p$  diffraction reflection in the XRD pattern of the compositions under study as a function of annealing temperature ( $T_{\text{ann}}$ ). It is seen, the derivative  $d(\text{fwhm})/dT_{\text{ann}}$  is neither a constant nor monotonous function of  $T_{\text{ann}}$ . The fwhm value decreases faster in the vicinity of the respective transition temperature ranges.

Because of the specificity of formation (through quenching), as-prepared ceramics of HP-stabilized phases are under mechanical stress.<sup>18</sup> Annealing of the metastable phases releases the stress and, in some cases, even induces an irreversible transition(s) into other polymorph modification(s). The drop in the unit cell volume occurring as a result of the  $C2/c$ - $Pnma$  transformation certainly promotes the stress release.

The mechanical stress in the ceramics of  $\text{BiCrO}_3$  and  $\text{BiCr}_{0.9}\text{Sc}_{0.1}\text{O}_3$  is inhomogeneous. It follows from the general considerations: The ceramic grains are of irregular shape and characterized by a broad grain size distribution. Moreover, in addition to the intergranular cracks mentioned above, some intragranular cracks occurred as a result of annealing were also

observed. Figure 7 shows the SEM images of the same large grain (about 40  $\mu\text{m}$  in diameter) cracked during the annealing

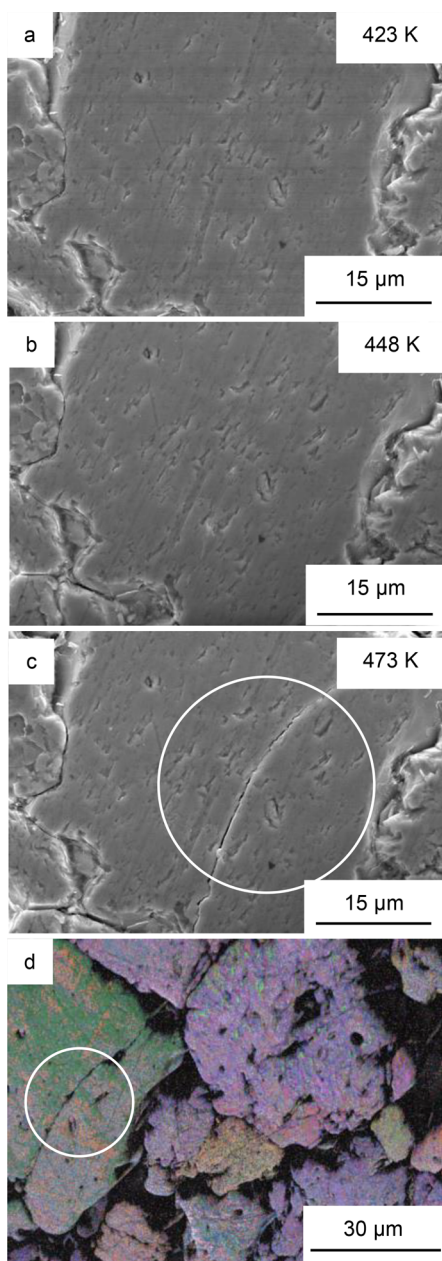


**Figure 7.** SEM images of the fragment of the same large grain ( $\sim 40$   $\mu\text{m}$  in diameter) of the  $\text{BiCrO}_3$  sample annealed at 423 K (a), 448 K (b), and 473 K (c). SEM image of surroundings of this grain after annealing at 473 K combined with an EBSD Euler map (d). The white circles show the same surface region in the micrographs. Different colors indicate different crystallographic orientations.

procedure with maximum temperature of 473 K, while after the procedure done at 448 K the grain was still intact. The EBSD Euler map that includes the surroundings of this grain is shown in Figure 7d. The Euler angle analysis indicates at least two different orientations in relation to a dominant axis in the large grain, suggesting competing stress fields.

Room-temperature PFM signal of the centrosymmetric monoclinic  $C2/c$  phase of  $\text{BiCrO}_3$  and  $\text{BiCr}_{0.9}\text{Sc}_{0.1}\text{O}_3$  was negligible, as expected. Nevertheless, after a scanning the  $\text{BiCrO}_3$  sample under negative or positive direct current (dc)

voltage applied to the PFM tip, a bipolar contrast appeared in PFM images (Figure 8). This contrast may be related either to

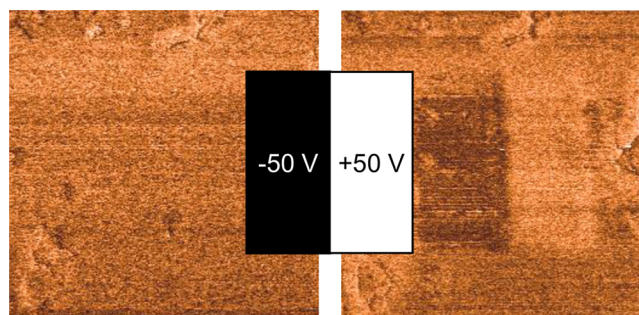


**Figure 8.** PFM response of the monoclinic phase of  $\text{BiCrO}_3$  before (left) and after (right) application of a dc voltage. The scan size is 10  $\mu\text{m}$ .

the induced piezoresponse that remains after the dc voltage is switched off or to electrical charges accumulated by the bias field during scanning. These charges (bulk of injected charge carriers) are trapped at defects in vicinity of the sample surface. When we deal with the surface charging, we can expect that on heating these trapped charges will be thermally activated and the induced PFM contrast will vanish. However, this was not the case. We observed that the PFM contrast remains upon heating and starts to disappear when approaching the transition temperature (Figure S3). Therefore, we may attribute the PFM signal to the piezoresponse of a polarized state induced by the application of an electric field. It should be mentioned that the field-induced transition from the antipolar to the polar state was reported for a similar composition  $\text{BiFe}_{0.5}\text{Mn}_{0.5}\text{O}_3$ <sup>23</sup> and was observed in the  $\text{BiFe}_{1-y}\text{Sc}_y\text{O}_3$  ceramics.<sup>24</sup> We attempted macroscopic polarization of the studied sample. However, samples quenched after the HP synthesis are fragile and have internal stresses as well as sizable conductivity. These factors resulted in breakdown of the sample already at moderate electric fields. Therefore, the macroscopic polarization tests by hysteresis measurements or second harmonic generation were impossible in our case and PFM has remained only the option to test the field-induced transition in these samples.

The local probe study was supplemented with the macroscopic dielectric measurements. Both compositions were found to demonstrate a broad dispersion and considerable dielectric losses. Nevertheless, the anomalies in both the real ( $\epsilon'$ ) and imaginary ( $\epsilon''$ ) parts of the complex dielectric permittivity were observed in the ranges of the phase transition of  $\text{BiCrO}_3$  and  $\text{BiCr}_{0.9}\text{Sc}_{0.1}\text{O}_3$  (Figures 9 and 10, respectively). While this anomaly is quite clearly seen for  $\text{BiCrO}_3$  ceramics, the respective dependence for  $\text{BiCr}_{0.9}\text{Sc}_{0.1}\text{O}_3$  is much more blurred by electrical conductivity effects. In addition to the net conductivity, charge accumulation at the grain boundaries, cracks, or imperfections occur, which lead to so-called Maxwell–Wagner–Sillars relaxation and increase the total conductivity. We believe that this is the main reason why  $\text{BiCr}_{0.9}\text{Sc}_{0.1}\text{O}_3$  is much more conductive, especially at temperatures above the phase transition point.

Both compositions exhibit dielectric relaxation in a low-temperature range. The dispersive shoulder in  $\epsilon'(T)$  and frequency-dependent maxima in  $\epsilon''(T)$  are seen although they are rather masked in  $\text{BiCr}_{0.9}\text{Sc}_{0.1}\text{O}_3$  because of the above-mentioned conductivity contribution to the total dielectric

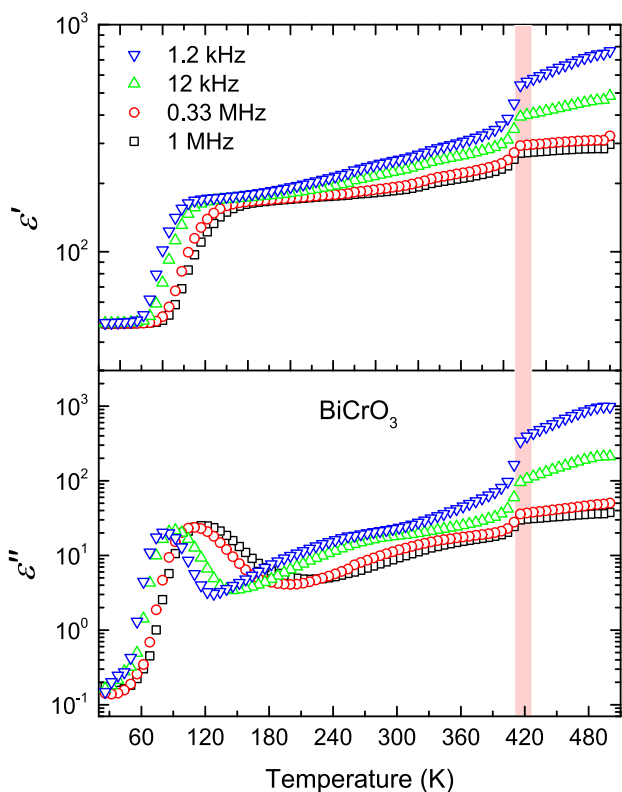


**Figure 9.** Temperature dependence of the real part (top) and the imaginary part (bottom) of the complex dielectric permittivity of the  $\text{BiCrO}_3$  ceramics at different frequencies. The shadow zone corresponds to the transition temperature range.

response (cf. values of  $\epsilon''$  for  $\text{BiCrO}_3$  and  $\text{BiCr}_{0.9}\text{Sc}_{0.1}\text{O}_3$  in Figures 9 and 10). Such a low- $T$  dielectric relaxation has been observed in many compositions with oxygen-octahedral structure that contain bismuth at A-site.<sup>25–28</sup> Due to anisotropy of the  $6s^2(\text{Bi}^{3+})-2p^6(\text{O}^{2-})$  bond,  $\text{Bi}^{3+}$  cations are off-center displaced. The  $\text{Bi}^{3+}$  displacements induce local dipole moments, which are dynamic at relatively high temperatures. Slowing down of this dynamics on cooling results in the observed relaxation.

To extract more information about the dielectric behavior of  $\text{BiCrO}_3$  and  $\text{BiCr}_{0.9}\text{Sc}_{0.1}\text{O}_3$  in the vicinity of their phase transition temperatures, the electrical conductivity,  $\sigma = \omega\epsilon_0\epsilon''$ , (which is the main contributor to the total dielectric permittivity at these temperatures) of these ceramics was measured. The obtained data were fitted using the Almond–West formalism,<sup>29</sup> and the frequency-independent electrical conductivity (dc conductivity,  $\sigma_{\text{dc}}$ ) was extracted. Figure 11 shows a logarithm of  $\sigma_{\text{dc}}$  versus inverse temperature for both compositions studied. The values of activation energy ( $E_A$ ) were calculated using the Arrhenius law in the following form:

$$\sigma_{\text{dc}} = \sigma_0 \exp\left(-\frac{E_A}{kT}\right) \quad (1)$$

At temperatures above the phase transition into the orthorhombic phase, the values of activation energy for  $\text{BiCrO}_3$  and  $\text{BiCr}_{0.9}\text{Sc}_{0.1}\text{O}_3$  are similar: about 0.31 V for the unmodified composition and 0.34 eV for the Sc-substituted one (Figure 11). However, in the range of the monoclinic phase, those are 0.49 and 0.23 eV, respectively. Moreover, the  $Pnma-C2/c$  transition in  $\text{BiCrO}_3$  is accompanied by a decrease

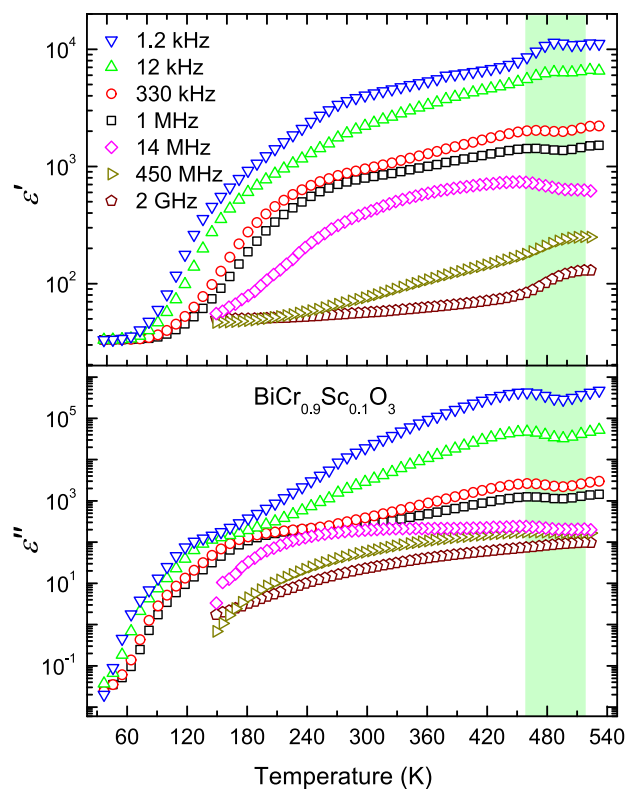


**Figure 10.** Temperature dependence of the real part (top) and the imaginary part (bottom) of the complex dielectric permittivity of the  $\text{BiCr}_{0.9}\text{Sc}_{0.1}\text{O}_3$  ceramics at different frequencies. The shadow zone corresponds to the transition temperature range.

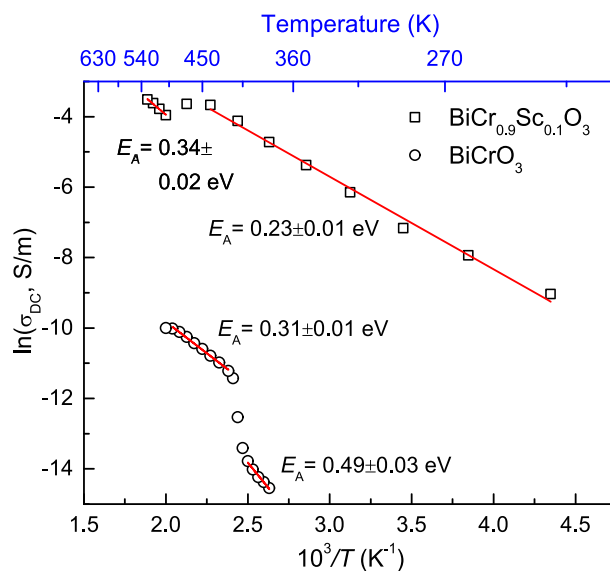


**Figure 11.** Log  $\sigma_{\text{dc}}$  vs  $10^3/T$  Arrhenius plots for the  $\text{BiCrO}_3$  and  $\text{BiCr}_{0.9}\text{Sc}_{0.1}\text{O}_3$  ceramics.

in the dc conductivity, while in  $\text{BiCr}_{0.9}\text{Sc}_{0.1}\text{O}_3$ ,  $\sigma_{\text{dc}}$  increases. Different  $\sigma_{\text{dc}}(T)$  behaviors of the unmodified and the Sc-substituted compositions at the phase transition is also seen from the temperature dependences of their dielectric responses (cf.: Figures 9 and 10: a negative and a positive change of  $\epsilon''$  upon cooling of the  $\text{BiCrO}_3$  and the  $\text{BiCr}_{0.9}\text{Sc}_{0.1}\text{O}_3$  ceramics,

respectively). The nature of such a difference is not clear and needs a particular study. The jump of the unit cell volume at the phase transition to the monoclinic phase is supposed to break some long-range routes for charge transport as it was evidenced by the microstructural study of the ceramics. However, the partial Cr-to-Sc substitution certainly promotes an easier charge transport. This is evident from bigger overall values of dc conductivity and the opposite change of the slope of the activation energy at the phase transition. The main problem, which can make difficult an investigation of mechanism(s) of the observed  $\sigma_{dc}(T)$  behaviors is that the microstructure changes caused by the phase transition in the  $\text{BiCrO}_3$  and the  $\text{BiCr}_{0.9}\text{Sc}_{0.1}\text{O}_3$  ceramics are unpredictable and irreversible.

Magnetic properties of the  $\text{BiCrO}_3$  ceramics prepared in this work were found to be very similar to those reported previously. According to the data of Belik et al.,<sup>11</sup> bismuth chromate orders magnetically below  $T_N \sim 111$  K and the curve of magnetization as a function of temperature exhibits two distinct regions. In the range between about 80 and 110 K, the net magnetization of  $\text{BiCrO}_3$  is low, while it increases to substantially higher values below 80 K. These magnetic transitions were studied with a neutron powder diffraction by Colin et al.<sup>30</sup> and it has been concluded that the lower temperature transition is a spin-reorientation, where antiferromagnetically coupled  $\text{Cr}^{3+}$  spins, initially aligned along the  $a$ -axis, rotate away from this direction staying in the  $(a, c)$  plane. In both the low- and high-temperature phases, the magnetic ordering remains G-type, which implies antiparallel alignment of the nearest neighbor spins.

We observed such a two-step increase of the magnetic susceptibility of the  $\text{BiCrO}_3$  sample below about 110 K (see inset in Figure 12). The values of the Néel temperature and the temperature of a spin reorientation transition ( $T_N \sim 110$  K and  $T_{sr} \sim 77$  K, respectively) were determined from the FC  $dM/dT$  versus  $T$  curve in the same manner as that reported by Belik<sup>11</sup> (Figure S4). The same  $T_N$  value was also found from

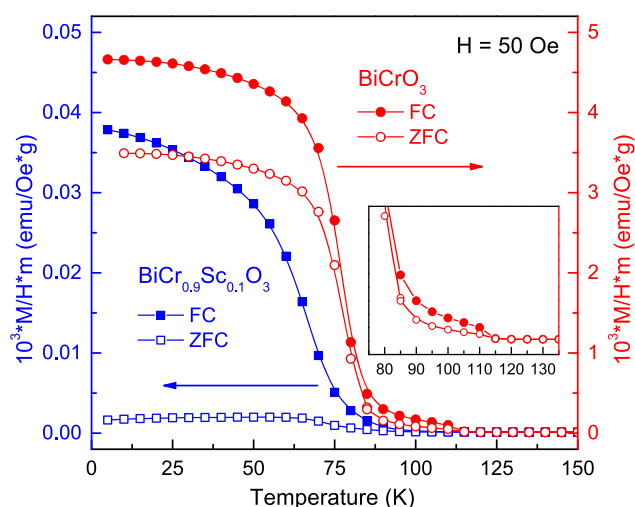


**Figure 12.** Low-temperature part of the temperature-dependent ZFC and FC static magnetic susceptibility of  $\text{BiCrO}_3$  (circles) and  $\text{BiCr}_{0.9}\text{Sc}_{0.1}\text{O}_3$  (squares). Notice the difference in scales associated with the respective data. Inset shows the temperature behavior of ZFC and FC static magnetic susceptibility of  $\text{BiCrO}_3$  in vicinity of the Néel temperature.

plots of the inverse ZFC and FC susceptibilities as a function of temperature (Figure S5).

The FC and ZFC magnetizations of  $\text{BiCr}_{0.9}\text{Sc}_{0.1}\text{O}_3$  were determined to be more than 2 orders of magnitude lower than those of  $\text{BiCrO}_3$  (Figure 12). The  $T_N$  value of  $\text{BiCr}_{0.9}\text{Sc}_{0.1}\text{O}_3$  was estimated from the plot of the inverse susceptibility versus temperature (Figure S6) to be about 85 K. In contrast to  $\text{BiCrO}_3$ , no sign was revealed of a two-step increase of the magnetic susceptibility upon cooling in  $\text{BiCr}_{0.9}\text{Sc}_{0.1}\text{O}_3$ . The magnetic properties of the  $\text{BiCr}_{0.9}\text{Sc}_{0.1}\text{O}_3$  sample are reminiscent of the unmodified  $\text{BiCrO}_3$  in the higher-temperature low-magnetization region.  $\text{BiCr}_{0.9}\text{Sc}_{0.1}\text{O}_3$  orders at substantially lower temperature ( $T_N \sim 85$  K), which is a result of the diamagnetic substitution of the B-site perovskite sublattice. In addition, unlike  $\text{BiCrO}_3$ , the Sc-substituted composition exhibits no spin-reorientation transition, and the state with the small net ferromagnetic moment is the ground state for this perovskite.

The origin of the ferromagnetic component in  $\text{BiCrO}_3$  was attributed by Colin et al.<sup>30</sup> to antisymmetric Dzyaloshinskii–Moria interaction. This assumption is fully consistent with the symmetry arguments coming from the representation theory used by the authors to classify transformational properties of different magnetic configurations with propagation vector  $\mathbf{k} = 0$ . The presence of the two temperature regions with lower and higher magnetization is however difficult to understand based on the spin reorientation within the  $(a, c)$  plane. The component of the Dzyaloshinskii–Moria vector, which couples the G-type antiferromagnetic and orthogonal ferromagnetic modes, is imposed by antiphase octahedral tilting.<sup>31,32</sup> In the monoclinic structure of  $\text{BiCrO}_3$ , the octahedral tilting occurs about the  $b$ -axis, implying that the relevant component of the Dzyaloshinskii–Moria vector is along this direction as well, and therefore, the spin reorientation should not affect the value of the spin canting within the  $(a, c)$  plane. Since the ground state of  $\text{BiCr}_{0.9}\text{Sc}_{0.1}\text{O}_3$  seems to be identical with the magnetic phase of  $\text{BiCrO}_3$  above 80 K, an additional neutron diffraction study of this composition might shed light on the anomalous magnetization behavior of the unmodified  $\text{BiCrO}_3$  perovskite.

#### 4. CONCLUSIONS

HP synthesis followed by quenching stabilizes  $\text{BiCrO}_3$  and  $\text{BiCr}_{0.9}\text{Sc}_{0.1}\text{O}_3$  in the perovskite structure with the same monoclinic  $C2/c$  symmetry at room temperature. A 10 mol %  $\text{Cr}^{3+}$ -to- $\text{Sc}^{3+}$  substitution in bismuth chromate results in an increase of the unit cell volume by about 1.3%. Both compositions exhibit a reversible phase transition from the monoclinic  $C2/c$  phase to the orthorhombic  $Pnma$  phase at 410–420 K ( $\text{BiCrO}_3$ ) and 490–520 K ( $\text{BiCr}_{0.9}\text{Sc}_{0.1}\text{O}_3$ ). A relative jump in volume of the perovskite primitive unit cell at the  $C2/c \rightarrow Pnma$  transition is  $-1.6$  and  $-2.0\%$  for unmodified and Sc-substituted compositions, respectively. The volume jump at the transition results in irreversible changes (cracking) in microstructure of the ceramics.

Application of a local electric field to the surface of the  $\text{BiCrO}_3$  ceramics in its centrosymmetric  $C2/c$  phase induces a polarized state that remains upon heating up to the transition temperature ranges.

Temperature-dependent complex dielectric permittivity of  $\text{BiCrO}_3$  and  $\text{BiCr}_{0.9}\text{Sc}_{0.1}\text{O}_3$  demonstrates broad dispersion and considerable dielectric loss and shows anomalies at their structural phase transition. The dc conductivity value jumps at the phase transition, and the sign of the jump is different for

unmodified and Sc-substituted compositions. The nature of such a difference is not clear and needs a particular study.

Both  $\text{BiCrO}_3$  and  $\text{BiCr}_{0.9}\text{Sc}_{0.1}\text{O}_3$  are antiferromagnetic below their Néel temperatures, which are 110 and 85 K, respectively. However, as opposed to the unmodified compound, the Sc-substituted one exhibits no spin reorientation transition.

## ■ ASSOCIATED CONTENT

### SI Supporting Information

The Supporting Information is available free of charge at <https://pubs.acs.org/doi/10.1021/acs.inorgchem.0c00338>.

XRD patterns recorded *in situ* between room temperature and 523 K, temperature derivatives of the FC and ZFC magnetization curves as a function of temperature, graphs of the inverse FC and ZFC susceptibility (PDF)

## ■ AUTHOR INFORMATION

### Corresponding Author

**Andrei N. Salak** – Department of Materials and Ceramics Engineering and CICECO – Aveiro Institute of Materials, University of Aveiro, 3810-193 Aveiro, Portugal; [orcid.org/0000-0001-5386-0280](https://orcid.org/0000-0001-5386-0280); Email: [salak@ua.pt](mailto:salak@ua.pt)

### Authors

**João Pedro Cardoso** – Department of Materials and Ceramics Engineering and CICECO – Aveiro Institute of Materials, University of Aveiro, 3810-193 Aveiro, Portugal; [orcid.org/0000-0002-4636-7831](https://orcid.org/0000-0002-4636-7831)

**Davide Delmonte** – Institute of Materials for Electronics and Magnetism, 43124 Parma, Italy; [orcid.org/0000-0001-5367-527X](https://orcid.org/0000-0001-5367-527X)

**Edmondo Gilioli** – Institute of Materials for Electronics and Magnetism, 43124 Parma, Italy

**Elena L. Fertman** – B. Verkin Institute for Low Temperature Physics and Engineering of NAS of Ukraine, 61103 Kharkov, Ukraine

**Alexey V. Fedorchenko** – B. Verkin Institute for Low Temperature Physics and Engineering of NAS of Ukraine, 61103 Kharkov, Ukraine

**Vladimir V. Shvartsman** – Institute for Materials Science and CENIDE – Center for Nanointegration Duisburg-Essen, University of Duisburg-Essen, 45141 Essen, Germany

**Vaidotas Paukšta** – Faculty of Physics, Vilnius University, LT-10222 Vilnius, Lithuania

**Robertas Grigalaitis** – Faculty of Physics, Vilnius University, LT-10222 Vilnius, Lithuania

**Jūras Banys** – Faculty of Physics, Vilnius University, LT-10222 Vilnius, Lithuania

**Dmitry D. Khalyavin** – ISIS Facility, Rutherford Appleton Laboratory, Didcot, Oxfordshire OX11 0QX, United Kingdom

**Joaquim M. Vieira** – Department of Materials and Ceramics Engineering and CICECO – Aveiro Institute of Materials, University of Aveiro, 3810-193 Aveiro, Portugal

Complete contact information is available at:

<https://pubs.acs.org/doi/10.1021/acs.inorgchem.0c00338>

### Notes

The authors declare no competing financial interest.

## ■ ACKNOWLEDGMENTS

J.P.C. acknowledges FCT – Fundação para a Ciência e Tecnologia, Portugal, for Ph.D. grant SFRH/BD/145281/

2019. The research performed in the University of Aveiro was developed within the scope of the project CICECO-Aveiro Institute of Materials, UIDB/50011/2020 & UIDP/50011/2020, financed by national funds through the FCT/MEC and when appropriate cofinanced by FEDER under the PT2020 Partnership Agreement.

## ■ DEDICATION

This work is dedicated to the memory of Dr. Vladimir Desnenko.

## ■ REFERENCES

- (1) Zheng, T.; Wu, J.; Xiao, D.; Zhu, J. Recent Development in Lead-Free Perovskite Piezoelectric Bulk Materials. *Prog. Mater. Sci.* **2018**, *98*, 552–624.
- (2) Dho, J.; Kim, W. S.; Chi, E. O.; Hur, N. H.; Park, S. H.; Ri, H. C. Colossal Magnetoresistance in Perovskite Manganite Induced by Localized Moment of Rare Earth Ion. *Solid State Commun.* **2003**, *125* (3–4), 143–147.
- (3) Cheong, S.-W.; Mostovoy, M. Multiferroics: A Magnetic Twist for Ferroelectricity. *Nat. Mater.* **2007**, *6* (1), 13–20.
- (4) Fu, H. Review of Lead-Free Halide Perovskites as Light-Absorbers for Photovoltaic Applications: From Materials to Solar Cells. *Sol. Energy Mater. Sol. Cells* **2019**, *193*, 107–132.
- (5) He, T.; Huang, Q.; Ramirez, A. P.; Wang, Y.; Regan, K. A.; Rogado, N.; Hayward, M. A.; Haas, M. K.; Slusky, J. S.; Inumara, K.; Zandbergen, H. W.; Ong, N. P.; Cava, R. J. Superconductivity in the Non-Oxide Perovskite  $\text{MgCNi}_3$ . *Nature* **2001**, *411* (6833), 54–56.
- (6) Belik, A. A.; Yi, W. High-Pressure Synthesis, Crystal Chemistry and Physics of Perovskites with Small Cations at the A Site. *J. Phys.: Condens. Matter* **2014**, *26* (16), 163201.
- (7) Sugawara, F.; Iiida, S.; Syono, Y.; Akimoto, S.-i. Magnetic Properties and Crystal Distortions of  $\text{BiMnO}_3$  and  $\text{BiCrO}_3$ . *J. Phys. Soc. Jpn.* **1968**, *25* (6), 1553–1558.
- (8) Goodenough, J. B.; Kafalas, J. A.; Longo, J. M. High-Pressure Synthesis. In *Preparative Methods in Solid State Chemistry*; Hagemuller, P., Ed.; Elsevier, 1972; pp 1–69.
- (9) Johnson, R. D.; Mezzadri, F.; Manuel, P.; Khalyavin, D. D.; Gilioli, E.; Radaelli, P. G. Evolution of Magneto-Orbital Order Upon B-Site Electron Doping in  $\text{Na}_{1-x}\text{Ca}_x\text{Mn}_2\text{O}_{12}$  Quadruple Perovskite Manganites. *Phys. Rev. Lett.* **2018**, *120* (25), 257202.
- (10) Shimakawa, Y. A-Site-Ordered Perovskites with Intriguing Physical Properties. *Inorg. Chem.* **2008**, *47* (19), 8562–8570.
- (11) Belik, A. A. Magnetic Properties of Solid Solutions between  $\text{BiCrO}_3$  and  $\text{BiGaO}_3$  with Perovskite Structures. *Sci. Technol. Adv. Mater.* **2015**, *16* (2), 026003.
- (12) Salak, A. N.; Shilin, A. D.; Bushinski, M. V.; Olekhovich, N. M.; Vyshatko, N. P. Structural Regularities and Dielectric Phenomena in the Compound Series  $\text{PbB}^{3+}_{1/2}\text{Nb}_{1/2}\text{O}_3$ . *Mater. Res. Bull.* **2000**, *35* (9), 1429–1438.
- (13) Niitaka, S.; Azuma, M.; Takano, M.; Nishibori, E.; Takata, M.; Sakata, M. Crystal Structure and Dielectric and Magnetic Properties of  $\text{BiCrO}_3$  as a Ferroelectromagnet. *Solid State Ionics* **2004**, *172* (1–4), 557–559.
- (14) Belik, A. A.; Iikubo, S.; Kodama, K.; Igawa, N.; Shamoto, S.; Takayama-Muromachi, E. Neutron Powder Diffraction Study on the Crystal and Magnetic Structures of  $\text{BiCrO}_3$ . *Chem. Mater.* **2008**, *20* (11), 3765–3769.
- (15) Darie, C.; Goujon, C.; Bacia, M.; Klein, H.; Toulemonde, P.; Bordet, P.; Suard, E. Magnetic and Crystal Structures of  $\text{BiCrO}_3$ . *Solid State Sci.* **2010**, *12* (5), 660–664.
- (16) Singh, A.; Singh, V. N.; Canadell, E.; Íñiguez, J.; Diéguez, O. Polymorphism in Bi-Based Perovskite Oxides: A First-Principles Study. *Phys. Rev. Mater.* **2018**, *2* (10), 104417.
- (17) Belik, A. A.; Iikubo, S.; Kodama, K.; Igawa, N.; Shamoto, S. I.; Maie, M.; Nagai, T.; Matsui, Y.; Stefanovich, S. Y.; Lazoryak, B. I.; et al.  $\text{BiScO}_3$ : Centrosymmetric  $\text{BiMnO}_3$ -Type Oxide. *J. Am. Chem. Soc.* **2006**, *128* (3), 706–707.

(18) Khalyavin, D. D.; Salak, A. N.; Fertman, E. L.; Kotlyar, O. V.; Eardley, E.; Olekhnovich, N. M.; Pushkarev, A. V.; Radyush, Y. V.; Fedorchenko, A. V.; Desnenko, V. A.; et al. The Phenomenon of Conversion Polymorphism in Bi-Containing Metastable Perovskites. *Chem. Commun.* **2019**, *55* (32), 4683–4686.

(19) Salak, A. N.; Khalyavin, D. D.; Pushkarev, A. V.; Radyush, Y. V.; Olekhnovich, N. M.; Shilin, A. D.; Rubanik, V. V. Phase Formation in the  $(1-y)\text{BiFeO}_3-y\text{BiScO}_3$  System under Ambient and High Pressure. *J. Solid State Chem.* **2017**, *247*, 90–96.

(20) Rodríguez-Carvajal, J. Recent Advances in Magnetic Structure Determination by Neutron Powder Diffraction. *Phys. B* **1993**, *192* (1–2), 55–69.

(21) Salak, A. N.; Khalyavin, D. D.; Mantas, P. Q.; Senos, A. M. R.; Ferreira, V. M. Structure-Dependent Microwave Dielectric Properties of  $(1-x)\text{La}(\text{Mg}_{1/2}\text{Ti}_{1/2})\text{O}_3-x\text{La}_{2/3}\text{TiO}_3$  Ceramics. *J. Appl. Phys.* **2005**, *98* (3), 034101.

(22) Ding, J.; Wen, L. W.; Kang, X. B.; Li, H. D.; Zhang, J. M. Polar and Nonpolar Structures of  $\text{BiCrO}_3$  from First-Principles Calculations. *Comput. Mater. Sci.* **2015**, *96* (A), 219–222.

(23) Delmonte, D.; Mezzadri, F.; Gilioli, E.; Solzi, M.; Calestani, G.; Bolzoni, F.; Cabassi, R. Poling-Written Ferroelectricity in Bulk Multiferroic Double-Perovskite  $\text{BiFe}_{0.5}\text{Mn}_{0.5}\text{O}_3$ . *Inorg. Chem.* **2016**, *55* (12), 6308–6314.

(24) Shvartsman, V. V. Progress report on microstructure/local properties measurements. Deliverable D6.3 for Project TUMOCs Grant Agreement No 645660; EU HORIZON 2020 MSCA-RISE-2014 programme, 2014. <https://ec.europa.eu/research/participants/documents/downloadPublic?documentIds=080166e5b36b7503&appId=PPGMS>.

(25) Nino, J. C.; Lanagan, M. T.; Randall, C. A. Dielectric Relaxation in  $\text{Bi}_2\text{O}_3\text{-ZnO-Nb}_2\text{O}_5$  Cubic Pyrochlore. *J. Appl. Phys.* **2001**, *89* (8), 4512–4516.

(26) Wang, H.; Kamba, S.; Du, H.; Zhang, M.; Chia, C. T.; Veljko, S.; Denisov, S.; Kadlec, F.; Petzelt, J.; Yao, X. Microwave Dielectric Relaxation in Cubic Bismuth Based Pyrochlores Containing Titanium. *J. Appl. Phys.* **2006**, *100* (1), 014105.

(27) Salak, A. N.; Ferreira, V. M.; Vieira, L. G.; Ribeiro, J. L.; Pullar, R. C.; Alford, N. M. Dielectric Relaxation and Microwave Loss in the  $\text{La}(\text{Mg}_{1/2}\text{Ti}_{1/2})\text{O}_3\text{-(Na}_{1/2}\text{Bi}_{1/2})\text{TiO}_3$  Perovskite Ceramics. *J. Mater. Res.* **2007**, *22* (10), 2676–2684.

(28) Salak, A. N.; Ferreira, V. M.; Ribeiro, J. L.; Vieira, L. G.; Pullar, R. C.; Alford, N. M. Bismuth-Induced Dielectric Relaxation in the  $(1-x)\text{La}(\text{Mg}_{1/2}\text{Ti}_{1/2})\text{O}_3-x\text{Bi}(\text{Mg}_{1/2}\text{Ti}_{1/2})\text{O}_3$  Perovskite System. *J. Appl. Phys.* **2008**, *104* (1), 014105.

(29) Almond, D. P.; West, A. R. Mobile Ion Concentrations in Solid Electrolytes from an Analysis of a.c. Conductivity. *Solid State Ionics* **1983**, *9–10*, 277–282.

(30) Colin, C. V.; Pérez, A. G.; Bordet, P.; Goujon, C.; Darie, C. Symmetry Adapted Analysis of the Magnetic and Structural Phase Diagram of  $\text{Bi}_{1-x}\text{Y}_x\text{CrO}_3$ . *Phys. Rev. B: Condens. Matter Mater. Phys.* **2012**, *85* (22), 224103.

(31) Khalyavin, D. D.; Salak, A. N.; Olekhnovich, N. M.; Pushkarev, A. V.; Radyush, Y. V.; Manuel, P.; Raevski, I. P.; Zheludkevich, M. L.; Ferreira, M. G. S. Polar and Antipolar Polymorphs of Metastable Perovskite  $\text{BiFe}_{0.5}\text{Sc}_{0.5}\text{O}_3$ . *Phys. Rev. B: Condens. Matter Mater. Phys.* **2014**, *89* (17), 174414.

(32) Khalyavin, D. D.; Salak, A. N.; Manuel, P.; Olekhnovich, N. M.; Pushkarev, A. V.; Radyush, Y. V.; Fedorchenko, A. V.; Fertman, E. L.; Desnenko, V. A.; Ferreira, M. G. S. Antisymmetric Exchange in La-substituted  $\text{BiFe}_{0.5}\text{Sc}_{0.5}\text{O}_3$  System: Symmetry Adapted Distortion Modes Approach. *Z. Kristallogr. - Cryst. Mater.* **2015**, *230* (12), 767–774.